Thermal dissipation of DIMM in Tower-BTX configuration

Giuseppe Petrone, Gaetano Sorge, Giuliano Cammarata
Department of Industrial and Mechanical Engineering University of Catania Viale A. Doria 6, 95125 Catania, Italy
E-mail: gpetrone@diim.unict.it, gcamma@diim.unict.it

ABSTRACT

Natural convection for Dual In-Line Memory Module (DIMM) systems, disposed as predicted by the recent Balanced Technology Extended (BTX) form factor in tower configuration, is numerically studied in this article. The considered physical system is modelled by horizontal air-filled layers bounded by parallel walls in which multiple heat sources are arranged. Three-dimensional simulations are carried-out by using a multi-physical FEM software. The results, obtained for imposed ambient temperature and operative conditions (power supplied to memories), show as thermo-convective instabilities may be produced and consequently complex fluid motion field could be detected. Simulated temperature fields show good agreement with thermal design data proposed by DIMM leading constructors. In order to improve computational performance of the numerical model, a simplified geometry is also proposed and tested for solving the physical problem. The present study contributes in investigation on critical cooling conditions for BTX form factor and in innovative projects of fan-less computer architecture.

NOMENCLATURE

C_p	isobaric specific heat	[J/(kg K)]
D_h	hydraulic diameter, $2LW/(L+W)$	[m]
$\vec{g}$	gravity acceleration	[m/s^2]
H	height of air volume	[m]
h	distance between circuit boards	[m]
k	thermal conductivity	[W/(m K)]
L	length of air volume	[m]
M	molecular mass of air	[kg/mole]
n	number of integrated circuits	
p	pressure	[Pa]
Q	thermal flux	[W]

q	specific thermal flux	[W/m^3]
R	Gas constant	[J/(kg mole)]
Ra	Rayleigh number, $gh^3 \Delta\rho / (\eta\alpha)$	
Re	Reynolds number, $\rho U D_h / \eta$	
T	temperature	[K]
t	time	[s]
$\vec{U}$	velocity vector, $(u,v,w)^t$	[m/s]
U	norm of velocity, $(u^2 + v^2 + w^2)^{1/2}$	[m/s]
W	width of air volume	[m]

Greek symbols

α	thermal diffusivity	[m^2/s]
η	dynamic viscosity	[Pa s]
ρ	density	[kg/m^3]
Ω	volume	[m^3]

Subscripts

a	ambient
C	chip
D	DIMM
P	printed circuit board

1. INTRODUCTION

Thermal design of electronic devices is an argument of high scientific, industrial and economic interest because of the primary importance that reliability and performance of those equipments cover in a very wide domain of technological applications. Electronic devices produce heat as a by-product of their normal operation. Besides the damage that heat may cause, it also increases the movement of free electrons in semiconductors, so that increasing in signal noise could be happen. When electronic devices are not efficiently cooled, the device junction temperature exceeds the maximum safe operating temperature specified by the manufacturer. Consequently, semiconductors performance, life, and reliability are drastically reduced [1-3]. As the result of a new approach to the thermal design of personal computers, Intel has recently developed the BTX form-factor (Balanced Technology eXtended), in order to replace the ATX case and motherboard layout. From a thermal point of view, the main specifics of the BTX form-factor consist in the in-line arrangement of high power components and in a thermal module able to force on those components an air-flow. Among the high power components, memories cooling system is one of the more sensitive subsystem in a BTX thermal design. Geometrically, this sub-system consists in a vertical or horizontal "channel" (depending on desktop or tower architecture of the machine) bounded by parallel memory modules in which the forced airflow is normally imposed [4]. However, this fluid flow is often disturbed by many factors. Cables, drive bays and brackets can determinate bypass over the memory components, forcing the subsystem to operate in natural convection. Therefore, natural convection represents a critical heat transfer mechanism assuring cooling for those components if forced airflow, for any reason, falls down. Otherwise, the passive character of cooling by natural convection makes it very attractive for possible application in electronic devices. From a

theoretical point of view, cooling of electronic packages has created emphasis on understanding the basic convective fluid flow over discrete heat sources, which have different characteristics from the traditionally studied convection from a heated whole wall [5]. On the other hand, most of the studies in the literature are regarding vertical channels [6-8] while only few investigations can be found concerning the heat transfer from discrete heat sources inside horizontal channels for air [9, 10]. DIMM are object of JEDEC standard and are made of a Printed Circuit Board (PCB) with multiple memory microchips displaced on it. They are connected to the circuit board by sockets and lateral guides [11]. Putting on our attention on BTX tower configuration, in which memory modules are horizontal, according to Infineon and Micron DIMM specifications about the opportunity of a CFD approach [12, 13], the present numerical study deals with multi-physical aspects concerning both thermal analysis of the solid components of the electronic devices (circuit board, socket, chip), and thermo-fluid-dynamical analysis of the fluid (air) surrounding the solid elements. Then, considering the expensive computational cost of a detailed 3D model, this paper also presents an adoptable strategy for obtaining a simplified numerical model.

2. NUMERICAL MODEL

Let consider the geometry reported in Figure 1. As shown, a twin set of four chips is overlapped on two horizontal circuit boards fixed in their backsides to a socket with lateral guides (left side of the Figure 1).

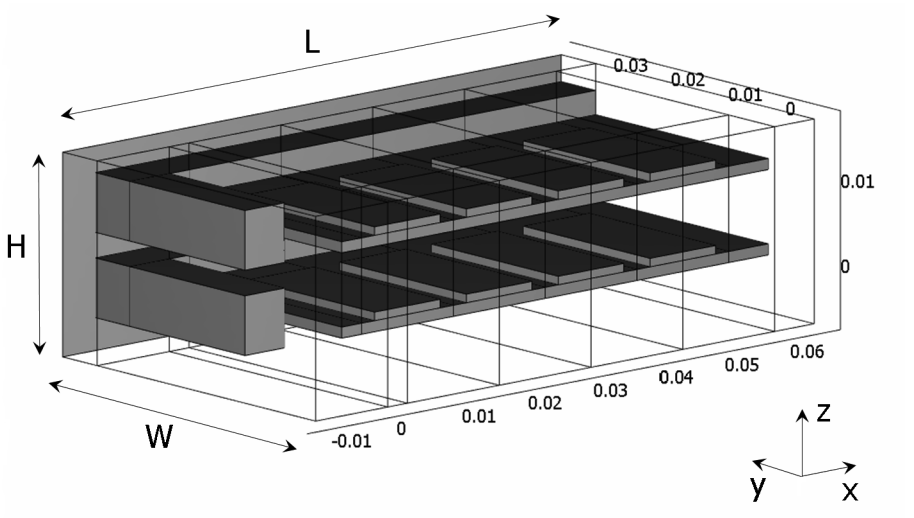

Figure 1 Geometry of the analyzed system.

The electronic devices stand in a surrounding air volume of length $L = 0.075$ [m], width $W = 0.044$ [m] and height $H = 0.024$ [m], respectively. The geometry reported in Figure 1 represents a half of a complete twin DIMM of 8 chip each one. Consequently, the y-z end-section, on the right of Figure 1, represents a geometrical symmetry section for the system. In natural convection, fluid is propelled by the buoyancy force, generated by a non-uniform density distribution due to local temperature gradients. In our problem, heating of fluid is related to the presence of heat sources (chips in operative conditions) plunged in the air

volume. The multi-physical problem is mathematically governed by conservation laws, the Navier-Stokes equations, characterizing flow of an incompressible fluid, and the energy equation, defining the equilibrium between heat fluxes (conductive one and convective one) and heat sources. The governing partial differential equations are reported in following:

$$\begin{cases} \rho\dfrac{\partial \vec{U}}{\partial t} + \vec{\nabla}\cdot(\rho\vec{U}\times\vec{U}) = -\vec{\nabla}p + \vec{\nabla}^2(\eta\vec{U}) + (\rho_0 - \rho)\vec{g} \\ \dfrac{\partial \rho}{\partial t} + \vec{\nabla}\cdot(\rho\vec{U}) = 0 \\ \rho C_p \dfrac{\partial T}{\partial t} + \vec{\nabla}\cdot(\rho C_p \vec{U}T) = q + \vec{\nabla}^2(kT) \end{cases} \quad (1)$$

The energy equation is solved in fluid as well as in solid sub-domains of system, by considering appropriate values for thermal conductivity ($k_C = 163$ [$Wm^{-1}K^{-1}$], $k_P = 0.3$ [$Wm^{-1}K^{-1}$]). Only in chip sub-domains the heat source term is different from zero and its value is $q = Q_D/(n_C\,\Omega_C)$. Adopted properties and conditions for fluid are reported in Table I.

Table I Dynamical and thermal properties of air.

Parameter	**Unit**
$M = 0.0288$	[$kg\ mol^{-1}$]
R = 8.134	[$J\ mole^{-1}kg^{-1}$]
$p_a = 101325$	[Pa]
$\rho \equiv p_0 M/(RT)$	[$kg\ m^{-3}$]
$\eta \equiv 6{,}0.10^{-6} + 4{,}0.10^{-8}T$	[Pas]
$k \equiv \exp(-3{,}723 + 0{,}865\ \log T)$	[$W\ m^{-1}K^{-1}$]
$C_P = 1100$	[$J\ kg^{-1}K^{-1}$]

Because of the particular technological interest of this kind of study, it seemed favourable solving conservation equations in their original dimensional form. This item allows to focus attention on the specific electronic device considered and make results directly exploitable by operators in this sector. Otherwise in multi-physical studying, where conservation equations are solved on both fluid and solid domains, classical dimensionless procedures involve not easy solution problems, as example the incongruent need of expressing a Prandtl number in energy equation for the solid domains. However, classical non dimensional groups are also used in post-processing of results. The Reynolds number, defined as $\mathrm{Re} \equiv \rho U D_h/\eta$, is evaluated basing on the hydraulic diameter of the bottom inlet section for air flow ($D_h = 2LW/(L + W)$), while the characteristic linear dimension adopted for Rayleigh number evaluation ($Ra \equiv gh^3\,\Delta\rho/(\eta\alpha)$) is the distance h between the overlapped circuit boards. Continuous conservation equations (1) are discretized by Finite Element Method on no-structured computational meshes, made of tetrahedral elements automatically generated by the used software (Comsol Multiphysics, v. 3.3). Then discrete equations are solved with following boundary conditions:

Fluid-dynamical conditions:

- No-slip conditions on interfaces between fluid and solid elements;
- Imposed pressure values on *x-y* boundaries of the fluid domain;
- Symmetry conditions on *y-z* end-section of the fluid domain;

Thermal conditions:

- Adiabatic for external walls of circuit boards and socket;
- Convective heat flux for top (*x-y*) and lateral (*y-z, x-z*) boundaries of the fluid domain;
- Imposed temperature for the bottom boundary of the fluid domain;

Time-integration of equations (1) has been performed for 2D approximation of the system only, in order to compare results of transient analysis with steady solution of conservation equations. Those results are discussed in the next section of this article. The temporal integration lies on a backward Euler method and the solver is an implicit time-stepping scheme solving a nonlinear system of equations at each time step [14]. In order to simplify the presentation of the adopted algorithm for steady solution of equations (1), let now indicate as $\vec{S} \equiv (\vec{U},\mathrm{T})^t$ a generic solution of Navier-Stokes and energy equations, and let consider the following assumptions for grouping transport, diffusion, buoyancy and pressure terms [15]:

$$[T\ (\vec{U})](\vec{S}) = -\begin{pmatrix} \vec{\nabla}\cdot(\rho\vec{U}\times\vec{U}) \\ \vec{\nabla}\cdot(\rho C_p\vec{U}T) \end{pmatrix}$$

$$D\ (\vec{S}) = \begin{pmatrix} \vec{\nabla}^2(\eta\vec{U}) \\ \vec{\nabla}^2(kT) \end{pmatrix}$$

$$B\ (\vec{S}) = \begin{pmatrix} (\rho_0 - \rho)\vec{g} \\ 0 \end{pmatrix}$$

$$[P\ (\vec{U})](\vec{S}) = -\begin{pmatrix} \vec{\nabla}p \\ 0 \end{pmatrix}$$

If $\vec{S}_0 \equiv (\vec{U}_0,\mathrm{T}_0)^t$ is a steady solution of equations (1) then it verifies the following expression:

$$[T\ (\vec{U}_0) + D + B + P\ (\vec{U}_0)](\vec{S}_0) = \vec{0} \tag{2}$$

An iterative approximation of steady state $\vec{S}_0$ by $\vec{S}^{(k+1)}$ is performed by applying a modified Newton-Raphson method [16], where a damping factor $0 < \lambda \leq 1$ is introduced in computing of perturbation, as in following:

$$\begin{cases} J_{T\ (\vec{U})+D+B+P\ (\vec{U})}[\vec{S}^{(k)}](\overrightarrow{\delta S}^{(k+1)}) = \\ -[T\ (\vec{U}^{(k)}) + D + B + P\ (\vec{U}^{(k)})](\vec{S}^{(k)}) \\ \vec{S}^{(k+1)} = \vec{S}^{(k)} + \lambda\overrightarrow{\delta S}^{(k)} \end{cases} \tag{3}$$

where the Jacobian operator $J_{T\ (\vec{U})+D+B+P(\vec{U})}$, expressed in $\vec{S}^{(k)}$ and applied to perturbation $\delta\vec{S}^{(k+1)}$, consists in difference between perturbed and not perturbed conservation equations linearized close to the $\vec{S}^{(k)}$ state. Once $\vec{S}^{(k+1)}$ evaluated, the relative error $E^{(k+1)}$ is computed as:

$$J_{T\ (\vec{U})+D+B+P\ (\vec{U})}(\vec{S}^{(k)})E^{(k+1)} = -[T\ (\vec{U}^{(k+1)})+D+B+P\ (\vec{U}^{(k+1)})](\vec{S}^{(k+1)}) \quad (4)$$

If $E^{(k+1)} > E^{(k)}$ then the code reduces the damping factor λ and computes $\vec{S}^{(k+1)}$ again. This algorithm repeats the damping-factor reduction until the relative error is less than in the previous iteration or until the damping factor underflows the imposed minimum value. When it has taken a successful step $\vec{S}^{(k+1)}$, the algorithm proceeds with the next Newton iteration. A value of λ =1 results in classical Newton's method, which converges quadratically if the initial guess is sufficiently close to the solution. The iterative procedure ends when:

$$\varepsilon = \left(\frac{1}{N} \sum_{i=1}^{N} \left(\frac{\left| E_i^{(k+1)} \right|}{\left| S_i^{(k+1)} \right|} \right)^2 \right)^{1/2} < \varepsilon_0$$

where N is the number of degrees of freedom for the system and ε_0, fixed at value 10^{-6} in this study, is an arbitrary small number. Algebraic systems coming from differential operators discretization are solved by using a direct unsymmetric multi-frontal method, particularly indicated in order to solve sparse matrix by LU decomposition. Computations have been carried-out on a 64 bit calculator of 16 GB of RAM. Influence of computational grid has been studied in order to assure mesh-independent results. In Table II we report a summary of the mesh studying. Relative gaps of maximum of temperature and velocity values over all the domains with respect to reference ones (evaluated for the finest tested grid) indicate that a mesh made of 24611 nodes (139857 d.o.f.) can be adopted assuring very small sensitivity of results with spatial discretization. Saturation of error with increasing in mesh refinement is otherwise well testified by Figure 2, where maximum of velocity is reported as function of the number of elements of the computational grid.

Table II Maximum values of temperature and velocity as function of the number of mesh elements and relative degrees of freedom. Relative gap with respect to reference values (values obtained for the finest grid) are also reported.

Elements	Increasing (%)	d.o.f.	T_{max} [°C]	Relative gap (%)	U_{max} [m/s]	Relative gap (%)
7052	-	38791	85.61	2.60	0.159	13.14
9871	40.0	55108	86.24	1.87	0.153	9.08
14128	43.1	79140	87.13	0.86	0.147	4.85
24611	74.2	139857	87.74	0.17	0.142	1.34
39536	60.6	225600	87.89	-	0.140	-

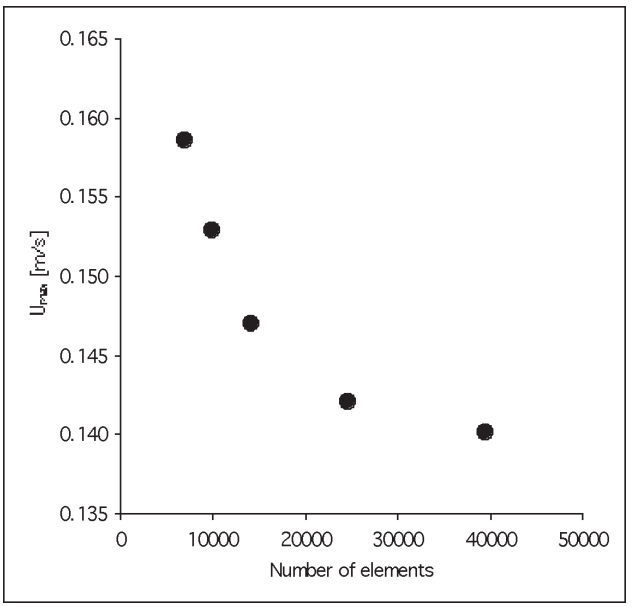

Figure 2 Maximum velocity values as function of the number of elements of the computational grid.

3. RESULTS

In this study we have been interested in simulating thermal and fluid-dynamical behaviour of the considered system. As known, 3D numerical models involve in very expensive computations, both for hardware and time needed for obtaining reliable results. Therefore, the goal of this study was at first reproducing physics of the considered system thought a detailed numerical model. Secondly, we spent attention in analyzing hypotheses able to simplify the numerical model, maintaining the same standard of result reliability with respect to accuracy assured by the more complex scheme. Simplification of physical system allows to drastically reduce degrees of freedom of the numerical model, so that memory space and computational time can be saved. The most part of results presented in this section come from solution of conservation equations in their steady formulation. The choice of solving system in steady condition arises from the idea of considering the technological devises in their thermal most unfavourable operative conditions, that consist in constant electrical load of alimentation equal to the maximum value indicated by technical documentation of their constructors. However, in order to validate the steady approach for solution, a comparison has been made between results obtained for 2D approximation both by transient and stationary analysis. Results presented in following are obtained for power supplied to DIMM $Q_D = 1\ W$ and for ambient temperature value $T_a = 30\ °C$. Figure 3 and Figure 4 show thermal fields and streamlines of flow, on a transversal section *y-z* (in correspondence of a couple of chip) of the geometry reported in Figure 1, evaluated by transient (Figure 3, t = 5200s) and steady (Figure 4) solution of equations (1), respectively. Topology of flow is quite identical for both cases: a primary motion field made of fluid flowing from the bottom boundary of the domain to the upper section turning around the solid domains, and a secondary motion

field characterized by the occurrence of a longitudinal convective roll developing in the semi-confined enclosure between the horizontal circuit boards. Drawn thermal levels also show good agreement each other, with a relative discrepancy for the maximum detected temperature of 0.84 %. Figure 5 reports velocity of fluid evaluated by transient analysis in three different geometrical points as function of time. It can be noted that, exceeded a transient time ($t \cong 3500$ s), the presented variables show a stationary behaviour. From 3D simulations the motion field of fluid appears more complex. As reported in Figure 6, where normalized velocity vectors are plotted in the x-z sections obtained for $y = 0.02$ and $y = 0.005$, the mean flow exhibits a pronounced chimney effect in correspondence of the central upper chips.

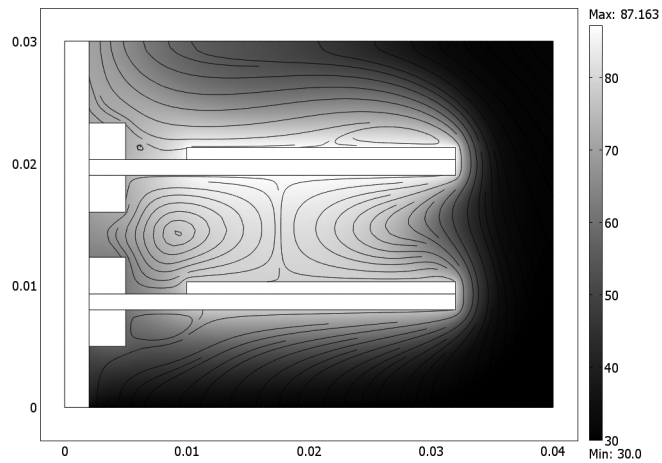

Figure 3 Thermal field and streamlines of flow for 2D transient (t=5200 s) solution of governing equations.

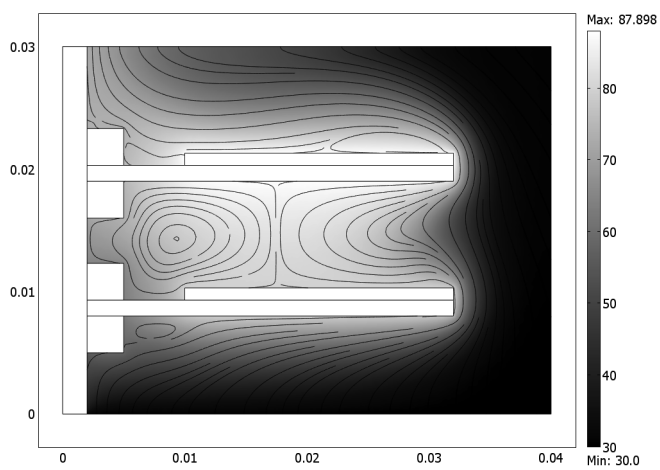

Figure 4 Thermal field and streamlines of flow for 2D steady solution of governing equations.

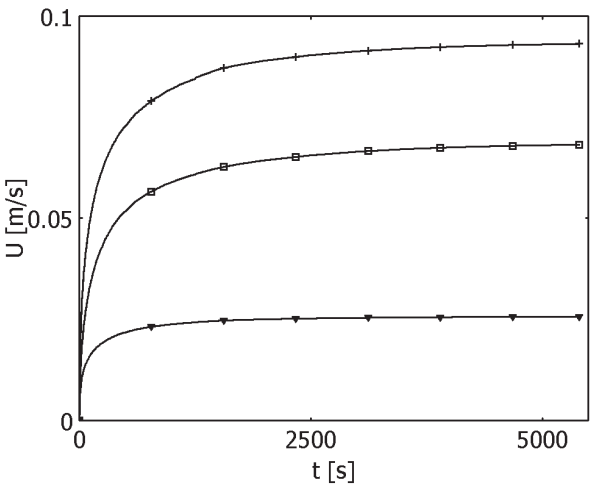

Figure 5 Velocity of fluid evaluated for $x = 0.04$ and $y = 0$ (triangle), $y = 0.01$ (square) and $y = 0.02$ (cross) as function of time.

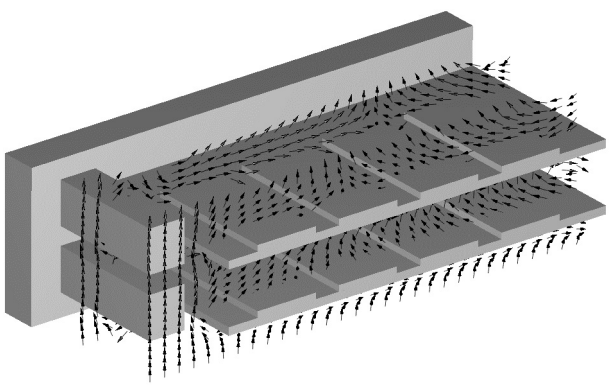

Figure 6 Normalized velocity vectors reported in x-z sections obtained for $y = 0.02$ and $y = 0.005$.

The internal flow maintains the longitudinal convective roll flow pattern highlighted by 2D analysis, but developing of thermo-convective instability is seen more articulated. In fact the re-circulation structure is not limited to the backside of the semi-confined cavity, but it also extends around the lateral bounds of the air volume comprised by the overlapped circuit boards. Extension of convective eddy over the lateral portions of volume, close to the lateral guides on the left side, and in correspondence of the symmetry section on the right side, is illustrated in Figure 7. Moreover, the convective structure assumes a helicoidally developing: fluid particles rotating around the longitudinal roll axis straightly shift along the axis direction. Transport direction mainly follows the way from the lateral guides to the transversal end-section of the geometry, where the convective eddy results more intensely

developed. From a thermal point of view, the elucidated flow pattern involves the following comments: the maximum value of temperature (T_{max} = 87.7°C) is detected in correspondence of the third chip standing on the upper circuit board, as illustrated in Figure 8 where thermal distribution on solid interfaces is plotted. Convective thermal flux reaches its maximum value close to the right top portion of the fluid volume. As a matter of fact, thermal energy produced inside the semi-confined control volume is worthy dissipated by the discussed dynamical roll, that transports and "ejects" it upward, very close to the top right corner of the fluid domain. The illustrated thermal fields well agree with the range of operative temperature indicated by leading DIMM constructors. In fact, in absence of forced airflow, and depending on the benchmark memory stress software applied, a temperature range of 75-95 °C is experimentally measured [13].

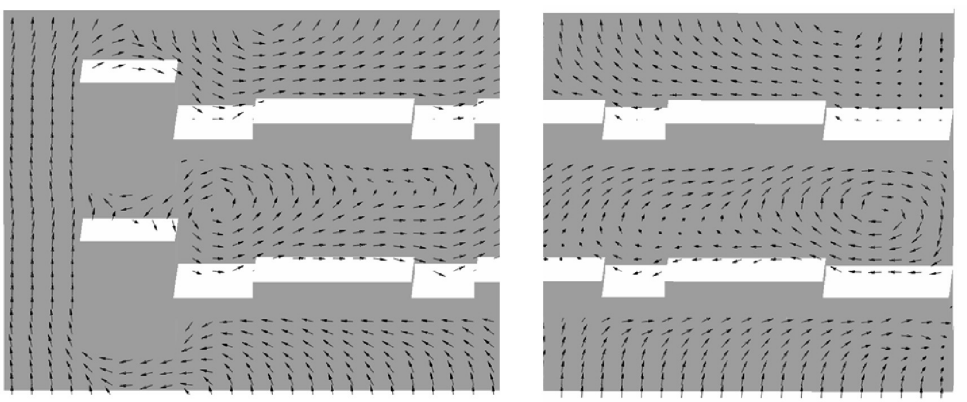

Figure 7 Frontal view of normalized velocity vectors reported in *x-z* sections obtained for $y = 0.018$.

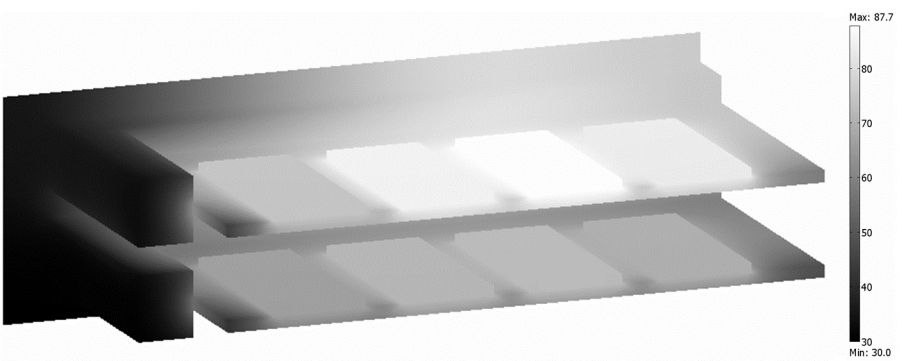

Figure 8 Thermal distribution on solid domains interfaces.

Once thermal and fluid dynamical fields obtained for a detailed model, the second objective of this study has been researching and testing a simplified model in order to reduce its degrees of freedom. The hypothesis that has been adopted consists in retaining that the sub-

domain simulating the sockets (in the backside of the system) could be suppressed without causing sensible variation in temperature distribution and velocity fields. Following this idea, a simplified model (Figure 9) giving, for the same level of mesh refinement, a number of d.o.f. of 93446 has been tested in order to replace the above discussed model (giving 139857 d.o.f.).

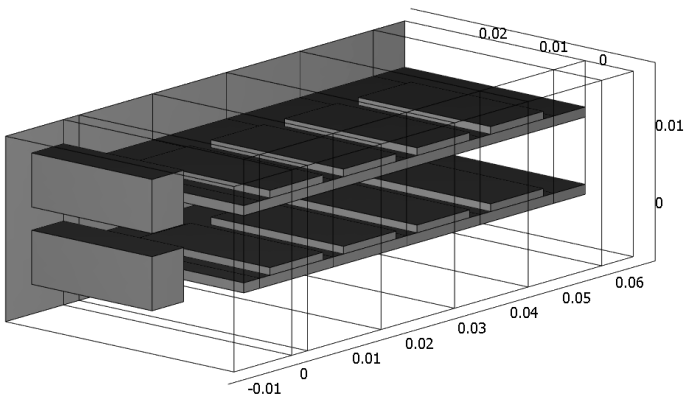

Figure 9 Geometry of simplified model.

In Table III a brief comparison between socket and no-socket model is proposed by reporting maximum values of velocity, temperature, Reynolds number and Rayleigh number obtained for both representations.

Table III. Comparison between socket and no-socket models.

	Socket	**No-Socket**	**Relative gap (%)**
U	0.142	0.154	8.31
T	87.7	87.9	0.18
Re	423	455	7.41
Ra	2205	2210	0.22

From a global point of view, thermal behaviour of system seems to be not very affected by model simplification, while dynamics appears more sensitive. However, in Figure 10 we report transversal *y-z* sections obtained for $x = 0.038$ where Ra is reported as field and velocity vectors are plotted in the semi-confined region bounded by the overlapped circuit boards. Vectors dimension is here proportionally related to the magnitude of velocity in order to assess its computed value for both cases. Highlighting secondary flow in the above mentioned spatial region of the system has made plotting of proportional vectors over all the fluid domain not favourable, due to the huge difference in magnitude between main flow and convective recirculation rolls. Suppression in fluid domain of the small sized enclosure due by sockets representation (right portion of the socket model reported in Figure 10) does not modify internal thermo-convective flow pattern. In fact, the secondary flow, assuring heat evacuation in the semi-confined region of the system, does not show any relevant

modification with respect to the complete model. Otherwise, in that spatial region, for both cases, the *Ra* number exceeds the critical value for the onset of classical Rayleigh-Bénard convective instabilities in differentially heated fluid layer. This item well agrees with the detected flow pattern reported for both models in Figure 10. Thermal analysis has also been performed in order to validate the simplified model. The maximum value of temperature all over the package is coherently obtained in correspondence of the third chip arranged on the upper circuit board. In Figure 11 evaluated temperature for the simplified model is reported as function of package length for $y = z = 0$. The almost horizontal portion of the plotted variable in Figure 11 correspond to detected temperature in correspondence of the integrated circuits. In the same figure the gap of reported values with respect to those computed at the same geometrical section for the complete model are also plotted.

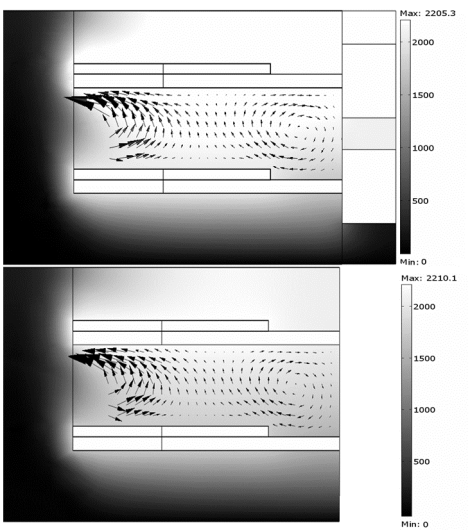

Figure 10 Rayleigh number distribution and velocity vectors in *y-z* sections obtained for $x = 0.038$ of the complete and the simplified model.

The maximum gap does not exceed 1.5 °C and it is detected on fluid domain, while temperature values evaluated on chip surfaces result quite identical. The obtained results globally confirm the validity of the simplifying hypothesis that allows to strongly save (30% about) computational time.

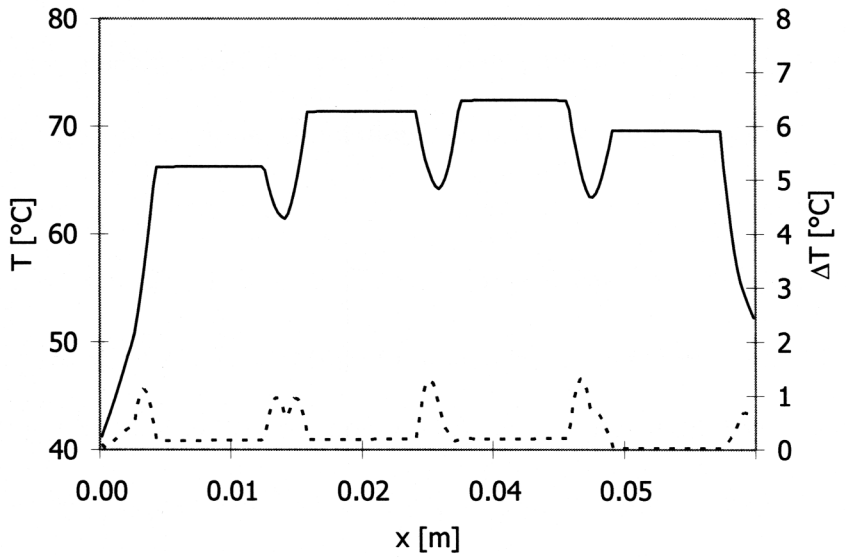

Figure 11 Temperature (left ordinate axis) as function of DIMM length evaluated for the simplified model for $y = z = 0$ (continuous line). Dashed line indicates gap (right ordinate axis) with respect to temperature computed by the complete model.

4. CONCLUSION

In this article a numerical study on thermal dissipation of DIMM in tower-BTX configuration is presented for natural convection conditions. The technological system is outlined by multiple heat sources arranged on two overlapped solid layers surrounded by air at rest conditions. Modelling and simulations have been conduced by using a FEM multi-physical software. Time-integration of two-dimensional conservation equations shows as, exceeded a transient period, the system assumes a time-independent thermal and fluid-dynamical behaviour, agreeing with results provided by direct solution of governing equations in their steady form. Detected temperature values by two-dimensional simulations are in accordance with experimental results supplied by leading constructors of the analysed technological devises. However, two-dimensional simulations only enable a partial view of real flow pattern and thermal transport effects. Indeed, from three-dimensional simulation it is seen that, in the spatial region bounded by the overlapped circuit boards, the onset of thermo-convective instabilities determinates a complex fluid flow. The convective roll is highlighted to assume a helicoidally rolling shape developing along lateral and backside space with respect to heat sources. That convective structure sensibly contributes in transport and dissipation of thermal energy produced in the horizontal semi-confined air volume. This study also provides a simplified approach in order to modelling the analysed electronic devices. From computed results it seems that suppression of sockets, and consequently modification in semi-confined air volume, very slightly influences dynamical and thermal fields of fluid. Otherwise thermal levels on solid domains result almost unaffected by the

assumed simplification in system modelling. Few three-dimensional numerical studies on this subject are actually presented in literature. For this reason, results provided in this paper could be helpfully exploited as scientific and technical tool for innovative projects of fan-less computers architecture.

REFERENCES

[1] C. Bailey, H. Lu, D. Wheeler, Computational modeling techniques for reliability of electronic components on printed circuit boards, *Applied Numerical Mathematics*, vol. 40 (2002), pp. 101-117.

[2] Hanreich G., Nicolics J., Musiejovsky L., High resolution thermal simulation of electronic components, *Microelectronics Reliability*, vol. 40 (2000), pp. 2069-2076.

[3] Towashiraporn P., Subbarayan G., McIlvanie B., Hunter B. C., Love D., Sullivan B., The effect of model building on the accuracy of fatigue life predictions in electronic packages, *Microelectronics Reliability*, vol. 44 (2004), pp. 115-127.

[4] El Alami M., Najam M., Semma E., Oubarra A., Penot F., Electronic components cooling by natural convection in horizontal channel with slots, *Energy Conversion and Management*, vol. 46 (2005), pp. 2762-2772.

[5] Bhowmik H., Tou K.W., Experimental study of transient natural convection heat transfer from simulated electronic chips, *Experimental Thermal and Fluid Science*, vol. 29 (2005), pp. 485-492.

[6] Harvest J., Fleischer A.S., Weinstein R.D., Modeling of thermal effects of heat generating devices in close proximity on vertically oriented printed circuit boards for thermal management applications, *International Journal of Thermal Sciences*, vol. 46 (2007), pp. 253-261.

[7] Bae H.J., Hyun J.M., Time-dependent buoyant convection in an enclosure with discrete heat sources, *International Journal of Thermal Sciences*, vol. 43 (2004), pp. 3-11.

[8] da Silva A.K., Lorenzini G., Bejan A., Distribution of heat sources in vertical open channels with natural convection, *International Journal of Heat and Mass Transfer*, vol. 48 (2005), pp. 1462-1469.

[9] Dogan A., Sivrioglu M., Baskaya S., Investigation of mixed convection heat transfer in a horizontal channel with discrete heat sources at the top and at the bottom, *International Journal of Heat and Mass Transfer*, vol. 49 (2006), pp. 2652-2662.

[10] da Silva A.K., Gosselin L., On the performance of an internally finned three-dimensional cubic enclosure in natural convection, *International Journal of Thermal Sciences*, vol. 44 (2005), pp. 540-546.

[11] JEDEC Technical Documentation, *http://www.jedec.com*.

[12] Balanced Technology Extended (BTX) System Design Guide 1.0, Intel Corporation (2004), *http://www.formfactors.org*.

[13] TN-00-08: Thermal Applications, Micron Technology Inc., vol. 2 (2004), *http://www.micron.com*.

[14] Brenan, K. E., Campbell, S. L., and Petzold, L. R., *Numerical Solution of Initial-Value Problems in Differential-Algebraic Equations*, Elsevier, New York (1989).

[15] Petrone G. Chénier E., Lauriat G., Stability of free convection in air-filled horizontal annuli: influence of the radius ratio, *International Journal of Heat and Mass Transfer*, vol. 47 (2004), pp. 3889-3907.

[16] P. Deuflhard, A modified Newton method for the solution of ill-conditioned systems of nonlinear equations with application to multiple shooting, *Numerical Mathematics*, vol. 22 (1974), pp. 289-315.